Mathematical Problems in Engineering
Volume 7, pp. 355–378
Reprints available directly from the publisher
Photocopying permitted by license only

A New Numerical Scheme for Non Uniform Homogenized Problems: Application to the Non Linear Reynolds Compressible Equation*

GUSTAVO C. BUSCAGLIA[a,†] and MOHAMMED JAI[b,‡]

[a]*Instituto Balseiro and Centro Atómico Bariloche, 8400, Bariloche, Argentina;* [b]*M.M.C.S., CNRS-UMR 5585, Insa de Lyon, Bat 401, 69621 Villeurbanne Cedex, France*

(Received 1 May 2000)

A new numerical approach is proposed to alleviate the computational cost of solving non-linear non-uniform homogenized problems. The article details the application of the proposed approach to lubrication problems with roughness effects. The method is based on a two-parameter Taylor expansion of the implicit dependence of the homogenized coefficients on the average pressure and on the local value of the air gap thickness. A fourth-order Taylor expansion provides an approximation that is accurate enough to be used in the global problem solution instead of the exact dependence, without introducing significant errors. In this way, when solving the global problem, the solution of local problems is simply replaced by the evaluation of a polynomial. Moreover, the method leads naturally to Newton-Raphson nonlinear iterations, that further reduce the cost.

The overall efficiency of the numerical methodology makes it feasible to apply rigorous homogenization techniques in the analysis of compressible fluid contact considering roughness effects. Previous work makes use of an heuristic *averaging* technique. Numerical comparison proves that homogenization-based methods are superior when the roughness is strongly anisotropic and not aligned with the flow direction.

Keywords: Compressible Reynolds lubrication equation; Taylor expansions; Numerical homogenized problems

---

*Dedicated to B. Alascio on his 60th birthday.

†e-mail: gustavo@cab.cnea.gov.ar

‡Corresponding author. Tel.: 33-72 43 8312, Fax: 33-72 43 8529, e-mail: jai@insa.insa-lyon.fr

1. INTRODUCTION

Homogenization techniques allow, under quite general hypotheses, to replace problems involving two (or more) very different scales by one macroscopic problem describing the mean behavior of the unknown field. The coefficients of this *homogenized equation* are calculated from local problems that account for the microscopic features. The aim is to avoid a huge numerical problem, with the global domain discretized finely enough so as to resolve the microscopic scale.

Difficulties arise, however, when trying to decouple the global and local problems in the presence of nonlinearities. In fact, the coefficients of the latter depend on the solution of the former, which in turn cannot be calculated until the coefficients of the homogenized equation are evaluated from the solution of local problems. This strong coupling appears, for example, in the homogenization of compressible flows under lubrication conditions, and its treatment is the subject of the present article. A typical technological application is the hard disk-reading head assembly, with length of about 5 mm and a surface-to-surface gap of 0.01 microns. These dimensions make it impossible to neglect roughness, that constitute the microscopic scale.

An alternative to homogenization techniques, when dealing with one-dimensional (longitudinal or transversal) roughness shapes, is the Film Thickness Averaging Method [10]. This method involves no local problems, but ambiguities appear when applying it to genuinely two-dimensional roughnesses. The usual way out of such ambiguities consists of heuristic combinations of one-dimensional formulae.

In the following we propose a numerical method that considerably reduces the number of local problems to be solved in a homogenization problem. The basic idea is the use of Taylor expansions for the evaluation of homogenized coefficients [6]. For the compressible Reynolds equation these depend, at any point x, on the mean gap $(H_0(x))$ and on the homogenized pressure $(P_0(x))$ as follows:

$$A^*(x) = A^*(H_0(x), P_0(x), w(H_0(x), P_0(x))) \tag{1}$$

where w is the solution of the local problem, that depends on $H_0(x)$ and $P_0(x)$. The main trick is to find a Taylor expansion for A^* as function of the two-vector $\alpha = (H_0, P_0)$, as this dependence can be shown to be smooth, and *not* as function of x.

The steps of the method are

- Choose a representative vector α^0 on the basis of reasonable estimates of H_0 and P_0. Select the order n of the Taylor expansion to be built around α^0.
- Solve the local problem to find *w and its derivatives with respect to* α up to order n at α^0.
- Calculate A^* *and its derivatives up to order* n at α^0 (expressions for the derivatives follow from the chain rule). Store the coefficients of the Taylor expansion.
- Solve the global homogenized problem, calculating the homogenized coefficients from their expansions, thus *not* solving local problems. Notice that this procedure decouples the global problem from the local ones.

The resulting algorithm leads to very low CPU costs, so that it becomes feasible to simulate general roughness shapes with homogenization techniques, which represent the fluid contact behaviour better than the Averaging Method.

Finally, let us remark that the exposition is restricted to quasi-periodic, steady problems. The quasi-periodicity assumption, that is, that the roughness is a small-scale periodic perturbation of an arbitrary reading head shape, is often invoked in two-scale analyses [3, 9]. In fact, stochastic rugosities are dealt with using similar theoretical tools in which the period is replaced by a *representative volume* [7]. In what concerns the steadiness assumption, this is certainly of intrinsic interest to evaluate the fluid contact behavior once transient effects have vanished. In addition, as shown in Ref. [8], dynamic coefficients (such as stiffness) can be inferred from steady analyses by perturbation techniques.

The plan of this article is as follows: In Section 2 two model problems are introduced, a linear one for which the method is most easily explained, and the compressible Reynolds equation modelling the flow of air between two rough surfaces (*i.e.*, the flying head and the hard disk). The third section deals with the numerical method. A more detailed mathematical analysis can be found in [5]. Section 4 contains the numerical method used for the global problem, and Section 5 shows several numerical examples, in particular a comparison with exact solutions available in 1D situations [6] and a strongly anisotropic

example in which the advantages of homogenization over Film Averaging are self evident.

2. DESCRIPTION OF THE HOMOGENIZED PROBLEMS

2.1. Linear Case

Consider the following Reynolds linear problem:

$$\begin{cases} -\nabla \cdot (H_\varepsilon^3 \nabla P_\varepsilon) = f & \text{in } \Omega \\ P_\varepsilon = 1 & \text{along } \partial\Omega \end{cases} \tag{2}$$

where $\Omega = \{x = (x_1, x_2) \in]0, 1[^2\}$. The function H_ε has the following form:

$$H_\varepsilon(x) = H_0(x) + H_1\left(\frac{x_1}{\varepsilon}, \frac{x_2}{\varepsilon}\right)$$

where ε is the roughness wavelength, that will tend to zero in the analysis and H_1 is a given ε-periodic function. When ε is very small, direct solution of (2) becomes prohibitively expensive. This difficulty is tackled by means of homogenization techniques [2, 6] briefly recalled in the following.

Introducing the (local) variables $y = (y_1, y_2) = ((x_1/\varepsilon), (x_2/\varepsilon))$ running over the unit cell $Y =]0, 1[\times]0, 1[$ and the asymptotic expansion

$$P_\varepsilon(x) = P_0(x) + \varepsilon P_1(x, y) + \varepsilon^2 P_2(x, y) + \cdots \tag{3}$$

where $P_1, P_2, \ldots$, are 1-periodic functions of the second variable. In the following, we note $H(x, y) = H_0(x) + H_1(y)$. Introducing the expansion (3) into Eq. (2) and using the differential rule:

$$\frac{\partial}{\partial x_i} = \frac{\partial}{\partial x_i} + \frac{1}{\varepsilon}\frac{\partial}{\partial y_i}$$

we obtain an expansion of differential operators with respect to ε^i. An identification of the leading term gives

$$-\nabla_y \cdot (H^3 \nabla_y P_1) = \nabla_x P_0 \cdot \nabla_y H^3 \quad \text{in } Y \tag{4}$$

$$\frac{\partial}{\partial x_1}\left[H^3\left(\frac{\partial P_0}{\partial x_1}+\frac{\partial P_1}{\partial y_1}\right)\right]+\frac{\partial}{\partial x_2}\left[H^3\left(\frac{\partial P_0}{\partial x_2}+\frac{\partial P_1}{\partial y_2}\right)\right]=-f+\nabla_y[\cdots] \tag{5}$$

To decouple the two equations above consider the local problems

$$-\nabla_y\cdot(H^3\nabla_y\omega_1)=\frac{\partial H^3}{\partial y_1} \quad \text{in } Y \tag{6}$$

$$-\nabla_y\cdot(H^3\nabla_y\omega_2)=\frac{\partial H^3}{\partial y_2} \quad \text{in } Y \tag{7}$$

where the unknowns ω_i, $i=1, 2$ are 1-periodic functions with respect to y. From (4) we get

$$P_1=\frac{\partial P_0}{\partial x_1}\omega_1+\frac{\partial P_0}{\partial x_2}\omega_2+C(x)$$

Replacement into (5) and integration over Y yields the homogenized problem

$$\begin{cases}-\nabla\cdot(A^*(H_0(x))\nabla P_0)=f & \text{in } \Omega\\ P_0=1 & \text{along } \partial\Omega\end{cases} \tag{8}$$

where $A^*(H_0(x))$ is a 2×2 matrix with components

$$\begin{cases}\tilde{A}^*_{ii}=\int_Y H^3\big((\partial\omega_i/\partial y_i)+1\big)dy & i=1,2\\ \tilde{A}^*_{12}=\int_Y H^3(\partial\omega_2/\partial y_1)dy\\ \tilde{A}^*_{21}=\int_Y H^3(\partial\omega_1/\partial y_2)dy\end{cases} \tag{9}$$

Remark 1 Notice that the ω_i are calculated numerically, and that they depend on x. This leads to a possibly large number of calculations for different values of x, that may be done without further modifications in parallel or, to alleviate the burden, by means of the method described in Section 3.

2.2. Non Linear Case

Air flow between the two surfaces constituting a rigid disk assembly (reading head and storage magnetic surface) is frequently approximed using the Reynolds equation. *For incompressible fluid, this approximation has been proved to be valid in* [1] *when the wavelength number is*

grater than the minimal gap. For compressible fluid, no rigorous proof exists but same kind of assumption is usually adopted [4]. Incorporating Burgdorfer's correction for very thin air gaps, the equation reads (upon normalization)

$$\frac{\partial}{\partial x_1}\left[(H^3P+6KH^2)\frac{\partial P}{\partial x_1}\right]+B^2\frac{\partial}{\partial x_2}\left[(H^3P+6KH^2)\frac{\partial P}{\partial x_2}\right]$$
$$=\Lambda_1\frac{\partial}{\partial x_1}(HP)+\Lambda_2\frac{\partial}{\partial x_2}(HP)$$
$$x=(x_1,x_2)\in\Omega=]0,1[\times]0,1[\quad P(x)=1\quad x\in\partial\Omega \tag{10}$$

where $H=(h/h_m)$ (h is the real gap and h_m the minimal gap) is the normalized gap thickness, $P=(p/p_a)$ (p is the real pressure and p_a the ambiant pressure) the normalized air pressure, K is the Knudsen number, $B=b/\ell$ (b: width of the reading head, ℓ: its length), and $\Lambda=(\Lambda_1,\Lambda_2)=(6\mu\ell/p_a h_m^2)U$ (μ is the air viscosity and U the surface velocity) the gas bearing number.

Actual magnetic surfaces are rough. In this case, the gap thickness function H is replaced by

$$H_\varepsilon(x)=H_0(x)+H_1\left(\frac{x_1}{\varepsilon},\frac{x_2}{\varepsilon}\right)$$

Using the same techniques as in the linear case one can obtain the following *homogenized problem* for the *homogenized pressure field* P_0

$$\begin{cases}\nabla\cdot(A^*(H_0(x),P_0(x))\nabla P_0)=\nabla\cdot(\Theta^*(H_0(x),P_0(x))P_0) & \text{in } \Omega\\ P_0=1 & \text{along } \partial\Omega\end{cases} \tag{11}$$

where the matrix A^* and the vector Θ^* are given by

$$\begin{cases}\tilde{A}^*_{ii}=((i-1)(B^2-1)+1)\\ \qquad\int_Y(H^3P+6KH^2)\big((\partial\omega_i/\partial y_i)+1\big)dy\quad i=1,2\\ \tilde{A}^*_{12}=\int_Y(H^3P+6KH^2)(\partial\omega_2/\partial y_1)dy\\ \tilde{A}^*_{21}=B^2\int_Y(H^3P+6KH^2)(\partial\omega_1/\partial y_2)dy\\ \tilde{\Theta}^*_1=\Lambda_1\int_Y\big(H+(H^3P+6KH^2)(\partial\chi_1/\partial y_1)\big)dy\\ \qquad+\Lambda_2\int_Y(H^3P+6KH^2)(\partial\chi_2/\partial y_1)dy\\ \tilde{\Theta}^*_2=B^2\Lambda_2\int_Y\big(H+(H^3P+6KH^2)(\partial\chi_2/\partial y_2)\big)dy\\ \qquad+B^2\Lambda_1\int_Y(H^3P+6KH^2)(\partial\chi_1/\partial y_2)dy.\end{cases} \tag{12}$$

and $\omega_i (i = 1, 2)$ and $\chi_i (i = 1, 2)$ are 1-periodic solutions of the following local problems (13) and (14)

$$L(H_0(x), P_0(x))\omega_i = ((i-1)(B^2-1)+1)\frac{\partial}{\partial y_i}(H^3 P_0 + 6KH^2) \tag{13}$$

$$L(H_0(x), P_0(x))\chi_i = ((i-1)(B^2-1)+1)\frac{\partial}{\partial y_i}(H) \tag{14}$$

Above, $L(H_0(x), P_0(x))$ stands for the operator

$$L(H_0(x), P_0(x))w = -\frac{\partial}{\partial y_1}\left[(H^3 P_0 + 6KH^2)\frac{\partial w}{\partial y_1}\right] - B^2\frac{\partial}{\partial y_2}\left[(H^3 P_0 + 6KH^2)\frac{\partial w}{\partial y_2}\right] \tag{15}$$

Remark 2 In this case, ω_i, χ_i depend also on P_0, which is the unknown of the global problem (11).

3. CALCULATION OF HOMOGENIZED COEFFICIENTS

The advantage of the homogenized problem (8) (resp. (11)) is eliminating the need for the global mesh to resolve the ε-scale, as is the case for the exact problem (2) (resp. (10)). On the other hand, if there exists no analytical solution to the local problems (as in the case of two-dimensional roughness), a very large number of local problems need be approximated on a partition of the unit cell (or local mesh). *Typically, if the global mesh consists of ND discretization points, the number of local problems to solve is* $4 \times ND$ *for the linear problem* (8)–(9) *and* $4 \times ND \times NIT$ *for the nonlinear problem* (11)–(12), *where NIT stands for the number of nonlinear iterations. As this number may reach several thousands, further algorithmic improvement is in order. One possibility to significantly reduce the complexity is described below. For clarity, the presentation deals with the linear model, but extension to the nonlinear case is straightforward.*

3.1. The Proposed Method in the Linear Case

The key idea comes from noticing that the multiple evaluations of A^* differ just in the values of $\alpha = H_0(x)$ intervening in (6)–(7). Though the

dependence of A^* on α is strongly implicit, techniques coming from sensitivity analysis allow for the construction of Taylor expansions on α.

We propose to replace A^* in (8) by its Taylor expansion of order n

$$T_{A_n^*}(\alpha) = A^*(\alpha_0) + \sum_{i=1}^{n} \frac{1}{i!} (\alpha - \alpha_0)^i \frac{\partial^i A^*(\alpha_0)}{\partial \alpha^i} \tag{16}$$

around some representative value α^0, so that, once the coefficients of the expansion are known, no further solution of a local problem is needed to evaluate A^* for an arbitrary value of α.

Remark 3 In the nonlinear case, problem (11), we consider a Taylor expansion of A^*, Θ^* with respect to $\alpha = (\alpha_1, \alpha_2) = (H_0(x), P_0(x))$:

$$T_{A_n^*}(\alpha) = A^*(\alpha^0) + \sum_{i=1}^{n} \frac{1}{i!} \left((\alpha_1 - \alpha_1^0) \frac{\partial}{\partial \alpha_1} + (\alpha_2 - \alpha_2^0) \frac{\partial}{\partial \alpha_2} \right)^i A^*(\alpha^0) \tag{17}$$

$$T_{\Theta_n^*}(\alpha) = \Theta^*(\alpha^0) + \sum_{i=1}^{n} \frac{1}{i!} \left((\alpha_1 - \alpha_1^0) \frac{\partial}{\partial \alpha_1} + (\alpha_2 - \alpha_2^0) \frac{\partial}{\partial \alpha_2} \right)^i \Theta^*(\alpha^0) \tag{18}$$

for a representative vector $\alpha^0 = (\alpha_1^0, \alpha_2^0)$.

3.2. Calculation of the Homogenized Coefficients

The method used to compute the derivatives intervening in (16) begins with the evaluation of the derivatives of the solutions ω_i of (6)–(7) up to the order n. The method proceeds as the following inductive sequence

Step 0 Solve the local problems (6)–(7).

Step 1 Computation of the following first derivatives

$$-\nabla_y \cdot \left(H^3 \nabla \frac{\partial w_i}{\partial \alpha} \right) = \frac{\partial}{\partial y_i} \left(\frac{\partial H^3}{\partial \alpha} \right) + \nabla_y \cdot \left(\frac{\partial H^3}{\partial \alpha} \nabla w_i \right) \text{ in } Y \tag{19}$$

Step 2 Calculation of second derivatives, the corresponding equations are obtained by differentiation of (19). The process continues up to the n-th order derivative.

Once the computation of all derivatives of ω_i up to order n has finished, those of A^* are obtained from the chain rule. The coefficient $\tilde{A}^*_{ii}$ and its derivative with respect to α are thus given by

$$\tilde{A}^*_{ii}(\alpha) = \int_Y (\alpha + H_1(y))^3 \left(\frac{\partial \omega_i}{\partial y_i} + 1 \right) dy \quad i = 1, 2$$

$$\frac{\partial \tilde{A}^*_{ii}}{\partial(\alpha)}(\alpha) = \int_Y 3(\alpha + H_1(y))^2 \left(\frac{\partial \omega_i}{\partial y_i} + 1 \right) dy + \int_Y (\alpha + H_1(y))^3 \frac{\partial}{\partial y_i} \left(\frac{\partial \omega_i}{\partial \alpha} \right) dy$$

$\tilde{A}^*_{12}$, $\tilde{A}^*_{12}$ are obtained analogously.

Remark 4 In the nonlinear case, problem (11), the coefficients depend on two parameters, $(\alpha_1, \alpha_2) = (H_0(x), P_0(x))$. The steps are the same, but the derivatives to evaluate are now with respect to both parameters.

4. GLOBAL PROBLEM IN THE NONLINEAR MODEL

Once the Taylor expansion coefficients of A^* and Θ^* have been calculated and stored (in a preprocessing stage), the evaluation of homogenized coefficients at quadrature points reduces to that of a polynomial expression. The impact on the CPU cost is evident. Moreover, notice that all derivatives of ω_i and ξ_i come out from linear systems where just the right-hand side is different. Only one matrix is to be assembled and factorized on the local mesh, and the calculation of an additional derivative increases the cost by a mere back-substitution. In fact, in [5] it was shown that Taylor expansions of fourth-order are accurate enough for practical purposes, so that the cost of the preprocessing stage is certainly very low and it becomes unnecessary to replace rigorous homogenization by heuristic formulae.

4.1. Newton-Raphson Iterations

Let us consider the homogenized nonlinear system (11). For its discretization, a finite-dimensional space $W_h \subset H^1(\Omega)$ is introduced.

We set

$$W_h^D = \{p_h \in W_h / p_{h|\partial\Omega} = 1\}$$

and

$$W_h^0 = \{p_h \in W_h / p_{h|\partial\Omega} = 0\}$$

The discrete version of (11) thus reads: *Find* $P_{0h}^{\Lambda} \in W_h^D$ *such that*

$$F(P_{0h}^{\Lambda}, q_h) = 0 \quad \forall q_h \in W_h^0 \tag{20}$$

where

$$F(P_{0h}^{\Lambda}, q_h) = \int_{\Omega} [A^*(H_0(x), P_{0h}^{\Lambda}(x)) \nabla P_{0h}^{\Lambda} \cdot \nabla q_h - \Lambda P_{0h}^{\Lambda}(x) \Theta^*(H_0(x), P_{0h}^{\Lambda}(x)) \cdot \nabla q_h] dx$$

A Newton-Raphson iteration to solve (20) thus reads

$$\begin{cases} 1. \text{ Let } P_{0h}^n \text{ be given in } W_h^D \\ 2. \text{ Find } \delta^n \in W_h^0 \text{ satisfying the linear system} \\ \quad D_1 F(P_{0h}^n, q_h) \cdot \delta^n = -F(P_{0h}^n, q_h) \ \forall q_h \in W_h^0 \\ 3. \text{ Set } P_{0h}^{n+1} = P_{0h}^n + \delta^n \text{ and go back to 1} \end{cases} \tag{21}$$

where $D_1 F$ is the derivative of F with respect to $\alpha_2 (= P_0(x))$ and is given by

$$\begin{aligned} D_1 F(P_{0h}^n, q_h) \cdot \delta^n = & \int_{\Omega} A^*(H_0(x), P_{0h}^n(x)) \nabla \delta^n \cdot \nabla q_h dx \\ & - \Lambda \int_{\Omega} \delta^n \Theta^*(H_0(x), P_{0h}^n(x)) \cdot \nabla q_h dx \\ & + \int_{\Omega} \delta^n \frac{\partial A^*}{\partial \alpha_2}(H_0(x), P_{0h}^n(x)) \nabla P_{0h}^n \cdot \nabla q_h \\ & - \Lambda \int_{\Omega} \delta^n \frac{\partial \Theta^*}{\partial \alpha_2}(H_0(x), P_{0h}^n(x)) P_{0h}^n \cdot \nabla q_h dx \end{aligned}$$

so that the derivatives of A^* and Θ^* with respect to P_0 are needed. At this point, if one has already constructed the Taylor expansions of A^* and Θ^*, one can simply differentiate them with respect to the second variable (α_2 in (17) and (18)) and in that way obtain the Taylor expansions of $(\partial A^*/\partial P_0)$ and $(\partial \Theta^*/\partial P_0)$.

4.2. Continuation Method

It is well known that, for Newton-Raphson's method to converge, the initial guess must be close enough to the solution. For that purpose, the following continuation method is used

(1) Let $\Lambda_0 = 0, \Lambda_1, \Lambda_2, \ldots, \Lambda_N = \Lambda$ be a subdivision of the interval $[0, \Lambda]$
(2) Let P_{0h}^0 be the solution of (20) obtained for $\Lambda = 0$
(3) For $i = 1$ to N the solution $P_{0h}^{\Lambda_i}$ of (20) is calculated by Newton-Raphson's iterations (21) using as initial-guess $P_{0h}^{\Lambda_{i-1}}$.

5. NUMERICAL TESTS

In this section the numerical solution of (11) is addressed. The proposed algorithm consists of two stages. In the first stage, the homogenized coefficients (12) and their derivatives up to order 4 at some parameter vector α^0 are calculated. This amounts to the solution of thirty problems of the type (13) (resp. (14)) to get ω_i (resp. χ_i) and their derivatives, differing in just the right-hand side. These problems are solved with Q_1 finite elements, employing 400 elements for the unit cell. The computing cost is small since the matrix is factorized only once. The second stage consists of solving the global problem (11) again by finite elements. We first consider an academic problem on a square domain to numerically assess the Taylor-expansion approximation for several roughness shapes. Convergence of the exact solution to the homogenized solution as ε tends to zero has been proved in [6]. Then we turn to a strongly anisotropic roughness and compare results obtained from both homogenization and film thickness averaging methods to a full-scale solution computed on a mesh that resolves the roughness scale and contains 250000? degrees of freedom. From the comparison it becomes evident that homogenization techniques have superior modelling capabilities.

5.1. Transversal Roughness

Let

$$H_0(x) = h_1 + (1 - h_1) * x_1$$
$$H_1(y) = \beta * (1 + \sin(2\pi y_1))$$

In [6] it is shown that the homogenized coefficients in this (transversal) case are given by

$$\begin{cases} A_{11}^* = (1/\int_0^1 (dy_1/(H_0(x)+H_1(y_1))^2 (H_0(x) \\ \qquad +H_1(y_1))P_0(x)+6K)) \\ A_{22}^* = \int_0^1 (H_0(x)+H_1(y_1))^2((H_0(x) \\ \qquad +H_1(y_1))P_0(x)+6K)dy_1 \\ \Theta_1^* = \int_0^1 (dy_1/(H_0(x)+H_1(y_1))((H_0(x) \\ \qquad +H_1(y_1))P_0(x)+6K))/ \\ \qquad \int_0^1 (dy_1/(H_0(x)+H_1(y_1))^2((H_0(x) \\ \qquad +H_1(y_1))P_0(x)+6K)) \\ A_{12}^* = A_{21}^* = \Theta_2^* = 0 \end{cases}$$

In Figures 1 to 5 we compare the numerical solutions obtained with these exact expressions for the coefficients (P^e) to those obtained with their Taylor expansions (17)–(18) around different points (P^t). The data are $h_1 = 10$, $\beta = 0.5$, $B = 13.25$, $K = 0.32$, $\Lambda = 3273$.

The physical constants from which the above normalized constants are derived are: $h_m = 0.2\,\mu$–m, $U = 20$ m/s; $l = 6.1$ mm, $b = 0.46$ mm, $\mu = 1.8110^{-5}$ Pa–s and $p_a = 1.01310^{-5}$ Pa.

In Figures 1, 3, 4, 6 and 9 we show contour lines of the homogenized pressure, at the bottom left corner of each graph the bearing number Λ and the extreme values of the solution can be found. The Taylor expansion is first taken around the point $\alpha^0 = (5, 1.5)$. It can be seen

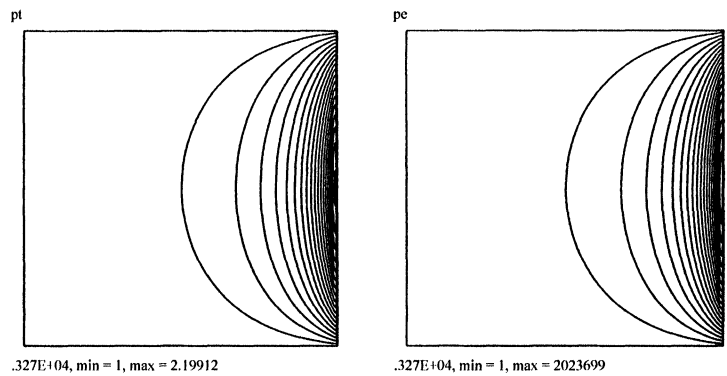

FIGURE 1 Comparison of the homogenized pressure calculated with the exact coefficients (P^e, at right), to that obtained with their Taylor expansions (P^t, at left): Contour lines. The selected value for α^0 is (5, 1.5).

that the contours of P^t and P^e are almost identical. The pressure profile along $x_2 = 0.5$ is shown in Figure 2. A boundary layer appears at the exit ($x_1 = 1$), and the mesh has consequently been refined there. The two profiles are practically indistinguishable, with a difference of 1.6% between the maximum value of p^e (2.23699) and of P^t (2.19912). We show below how to improve the accuracy increasing the number of points around which the Taylor expansion is performed.

Taking $\alpha^0 = (2, 1.5)$ the values of P^t change, the comparison with P^e can be seen in Figure 3, it becomes quite large if $\alpha^0 = (1.5, 1.5)$ (Fig. 4). Notice that the minimum pressure is 0.74, when the normalized pressure should always remain above 1.

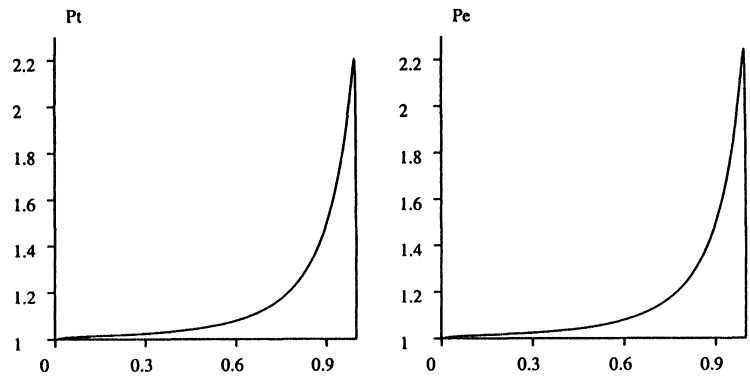

FIGURE 2 Same as Figure 1. Pressure profile along the central line $x_2 = 0.5$.

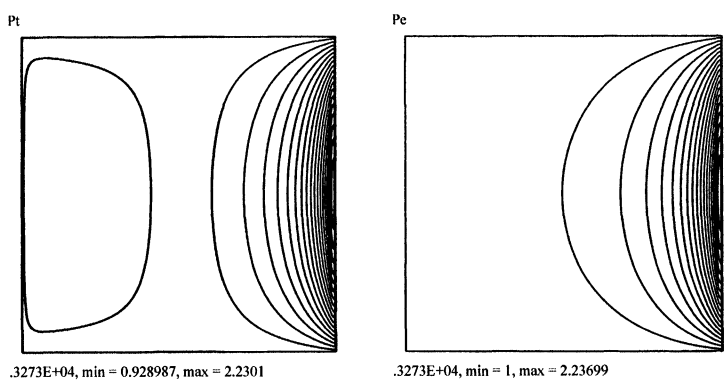

FIGURE 3 Same as Figure 1 for $\alpha^0 = (2, 1.5)$.

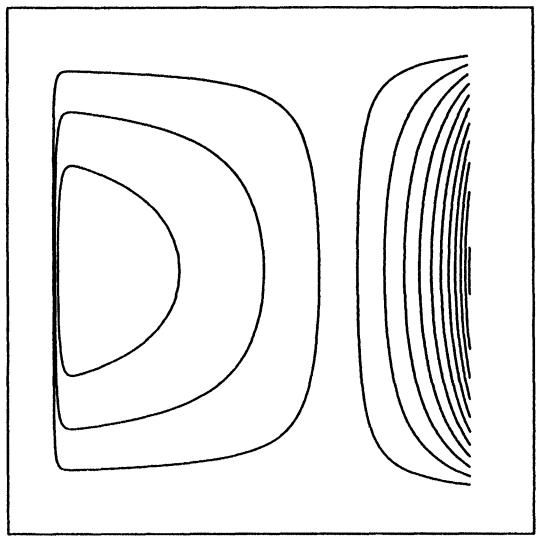

FIGURE 4 Same as Figure 1 for $\alpha^0 = (1.5, 1.5)$.

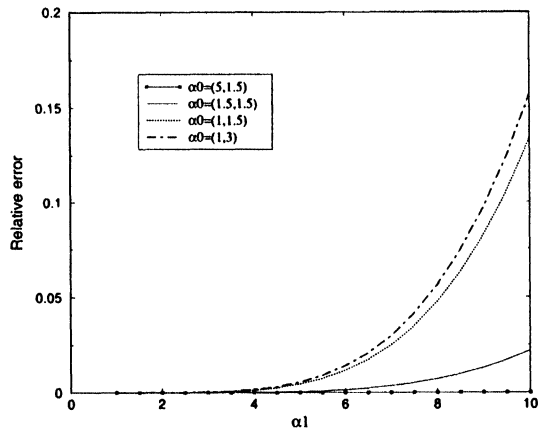

FIGUER 5 Error between the exact value of A^*_{11} and its fourth order Taylor expansions around several α^0, as a function of $\alpha_1 = H_0(x)$.

The errors that appear in Figures 3 and 4 are easily understood looking at Figure 5. There, the error between the exact coefficient A^*_{11} and its Taylor expansions of order four around several points α^0 are shown. It is clear that the difference is practically zero in $\alpha^0 = (5, 1.5)$ and grows as α^0 departs from this value.

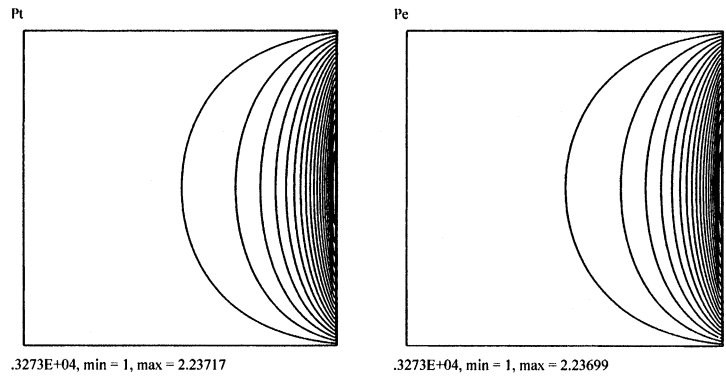

FIGURE 6 Same as Figure 1, using Taylor expansions around six points.

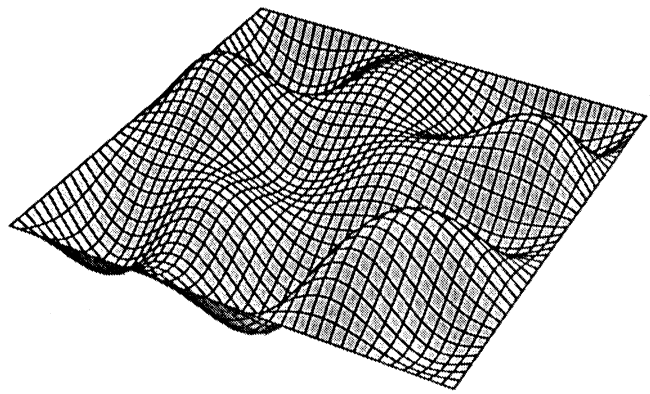

FIGURE 7 Randomly generated surface roughness on the unit cell.

The question thus arise as to how to select the appropriate α^0. The first component of α^0 represents $H_0(x)$, the air gap thickness, that varies between known bounds H_m and H_M. The second component is $P_0(x)$, that in practice varies between 1 and 10. The best choice consists of selecting several points in the α-parameter plane within the physically relevant region $[H_m, H_M] \times [0, 10]$. The number of points depends on the problem, for the cases considered we had excellent results using 6 points: ((1, 1), (1, 2), (2, 1), (2, 2), (4, 1) and (4, 2)). Notice that the Taylor expansions around these points can without any difficulty be calculated in parallel, as they are indepent from one another. Then, when a value of the coefficients is needed for some

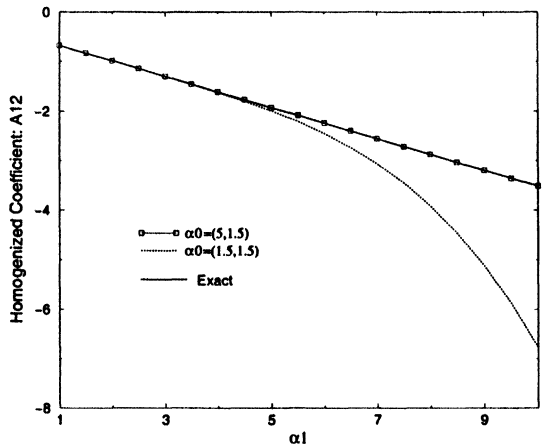

FIGURE 8 Homogenized coefficient A^*_{12} compared to its Taylor expansions for several values of α_0.

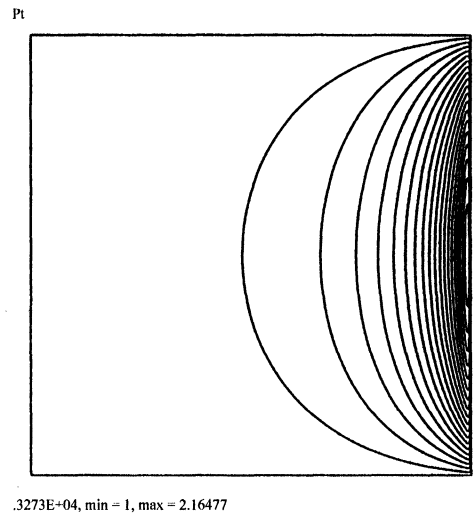

FIGURE 9 Pressure contours for the roughness function of Figure 7.

value of $H_0(x)$ and $P_0(x)$, it is evaluated from the Taylor expansion of the point among the six that is nearest. In this way the results of Figure 6 are obtained. The maximum is in this case 2.23717, with an error of 0.008% with respect to that of p^e (2.23699).

5.2. Randomly Generated Surface Roughness

The diffusion coefficient intervening in film thickness averaging methods [10] is diagonal. This is correct if the roughness is transversal, longitudinal, or in general orthotropic with axes aligned with the coordinate axes, but fails to be so in general roughness functions. To illustrate this, we solve Eq. (11) with the roughness function H_1 of Figure 7, corresponding to

$$H_1(y_1, y_2) = \sum_{i=1}^{m} \sum_{j=1}^{m} a_{i,j} \sin(\pi i y_1) \sin(\pi j y_2)$$

where $a_{i,j}$ is a randomly generated matrix. There exists no explicit expression for the homogenized coefficients in this case, so that solving local problems is unavoidable. The proposed method significantly reduces the number of local problems to be solved, but the cost is approximating the exact (implicit) dependence on $\alpha_1 = H_0$ and $\alpha_2 = P_0$ by a polynomial expression obtained from Taylor expansion. The error of this approximation is addressed in Figure 8, where A^*_{12} is plotted as function of α_1 taking $\alpha_2 = 2$. For comparison, the polynomials obtained by expansion around $\alpha^0 = (5,\ 1.5)$ and $\alpha^0 = (1.5,\ 1.5)$ are also plotted. Clearly the error of the former is much smaller than that of the latter, so that for this roughness the problem of selecting α_0 persists. It is solved with the same technique as before, and in fact using the same six points in parameter space. Another conclusion to be drawn from Figure 8 is that the extradiagonal component A^*_{12} is clearly different from zero, possibly leading to a prediction that differs significantly to that of averaging methods.

In view of the complexity of H_1 in (5.2) a finer mesh is needed for the local problem, in particular, for $m = 5$ (Fig. 7) 2500 elements are used in the unit cell. The physical data are taken the same as in the previous case.

The numerical tests put into evidence the ability of the method to handle complicated roughness functions without excessive computational burden. As an example, each problem in this section needed just 3 continuation steps to reach the final value of $\Lambda = 3273$, each of this steps converging in about 2 Newton-Raphson's iterations, with an overall computer cost of less than an hour in a RISC-based workstation. It should be mentioned that the mesh used for the global

problem consisted of 20000 bilinear quadrilateral finite elements (not shown because it is a black square when printed), allowing for an excellent resolution of internal and boundary layers.

5.3. Comparison of Homogenization and Film Thickness Averaging Methods for a Strongly Anisotropic Roughness

Let us now consider a more realistic slider configuration (see Fig. 10), with the following data taken from [10]: $l = 5.54\,\text{mm}$, $b = 0.513\,\text{mm}$, $l_r = 1.01\,\text{mm}$, $h_r = 10\,\mu\text{m}$, $h_c = -0.05\,\mu\text{m}$, $U = 20\,\text{m/s}$, $h_m = 0.15\,\mu\text{m}$ and $\delta = 0.2\,\mu\text{m}$. The roughness is discontinuous following a diagonal pattern shown in Figure 11. We computed three solutions to this problem. The first one, referred to as "homogenized" solution, was obtained applying the method proposed in the previous sections. The second one, referred to as "averaged" solution, was obtained applying the Film Thickness Averaging (FTA) method as detailed in [10]. Both

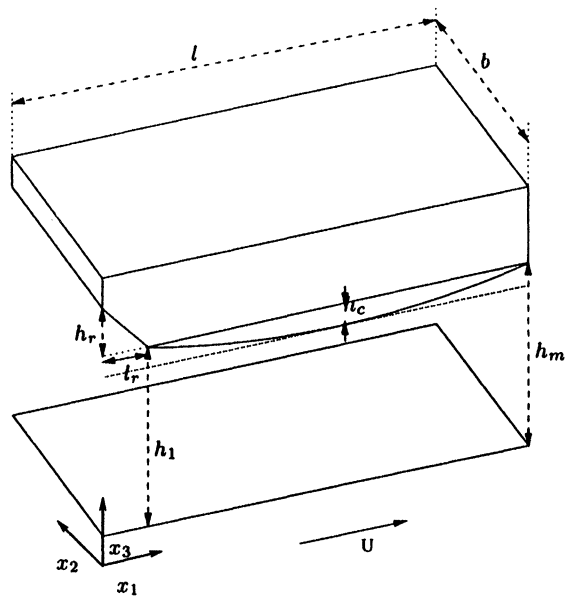

FIGURE 10 Taper flat slider configuration for magnetic disk use.

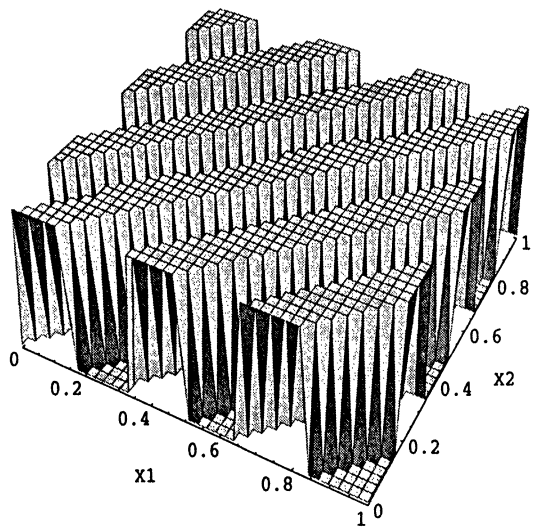

FIGURE 11 Slider with anisotropic roughness.

were calculated on the same mesh, consisting of 34911 nodes. To allow for comparison, a third solution was computed without averaging or homogenizing the roughness, considering $n_1 = 20$ roughness wavelengths in the longitudinal direction and $n_2 = 2$ roughness wavelengths in the transverse direction. The mesh for this computation must resolve the roughness scale, so that 64881 nodes are used. This latter solution is refered to as "exact" one.

For the selected conditions, especially due to the high anisotropy of the roughness shape that is not aligned with the flow, the homogenized and averaged solutions are very different, as can be observed in Figures 12 and 13. These are to be compared to the exact solution, of which a detail is shown in Figure 14. By direct inspection, it is clear that the symmetry predicted by the FTA method is not present in the exact solution, which qualitatively agrees mucy better with the homogenized solution. To get a more quantitative comparison, consider the pressure profiles along the longitudinal centreline (Fig. 15) and alone the transversal centreline (Fig. 16). Notice that the homogenized solution correctly approximates mean values of the exact solution, while the averaged pressure exhibits very poor agreement. If the number of roughness wavelengths is increased to

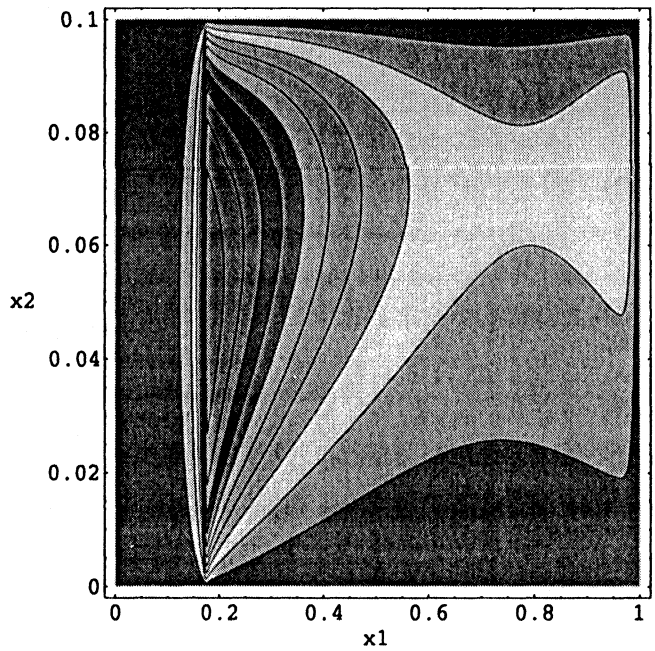

FIGURE 12 Homogenized pressure contours.

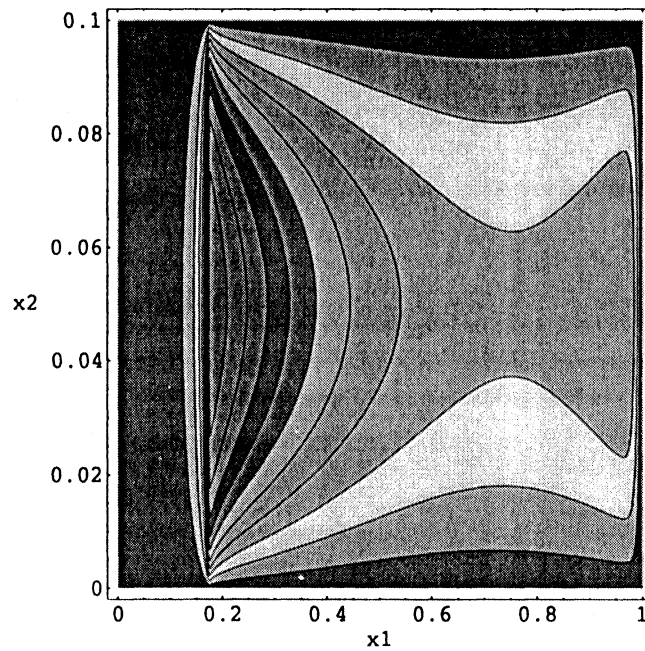

FIGURE 13 Averaged pressure contours.

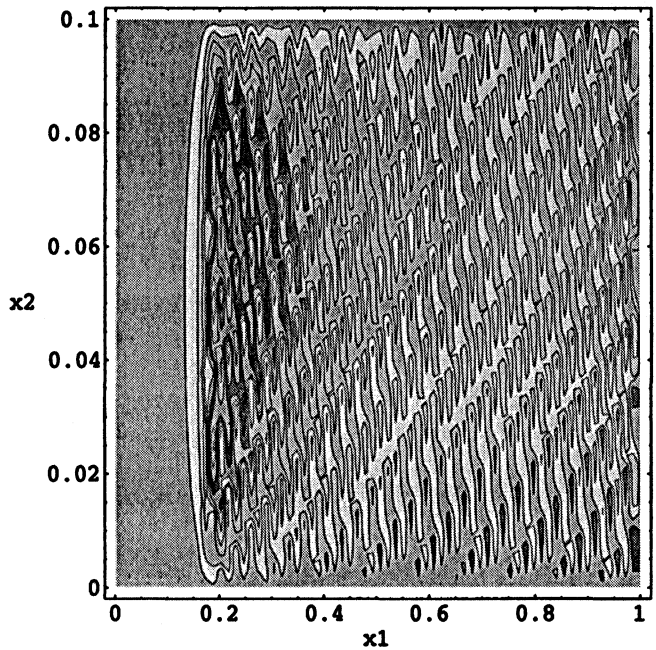

FIGURE 14 Exact pressure contours with $n_1 = 20$, $n_2 = 2$.

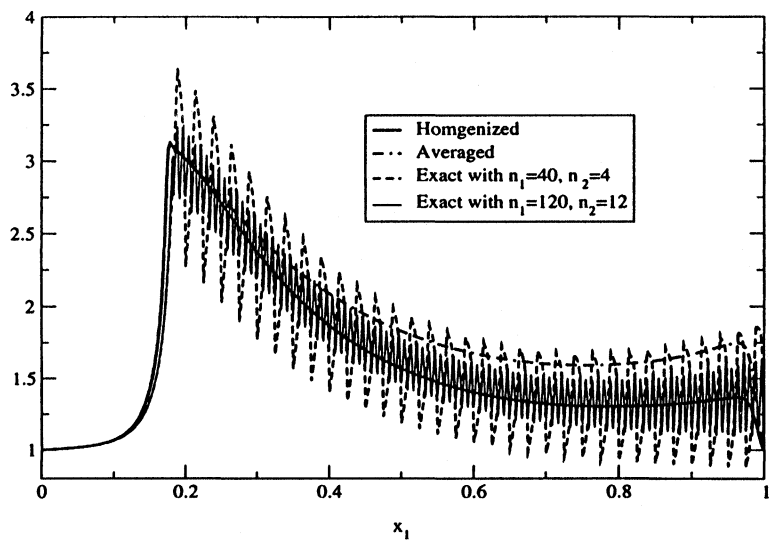

FIGURE 15 Exact, homogenized and averaged pressures at the middle of the rail.

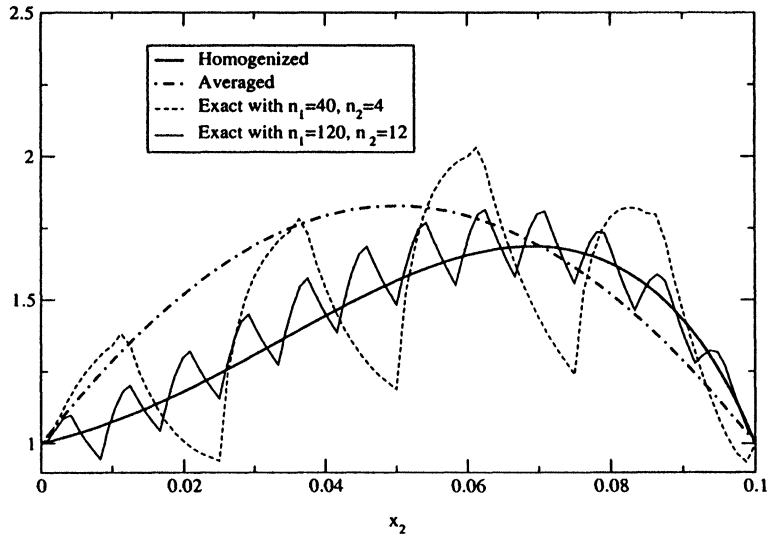

FIGURE 16 Exact, homogenized and averaged pressures at $x_1 = 0.5$.

$n_1 = 120$, $n_2 = 12$, it becomes evident that an accurate pressure field estimate is only provided by the homogenization technique.

We should remark, however, that in other roughness configurations such as checkerboard patterns (for which experimental results exist in [10]) the homogenized and averaged solutions are practically coincident and agree well with measured values. Also notice that the roughness shape of Figure 11 can be manufactured and that the lack of symmetry predicted in Figure 12 can be confirmed by experiments, since it leads to a non-vanishing torque around the longitudinal centreline.

6. FINAL REMARKS

Though the method has been described as if α^0 were unique, it is in fact preferable to calculate Taylor expansions around several values of α. This allows for the homogenized coefficients to be evaluated on the basis of an expansion around a point "that is not too far apart". Moreover, the difference between the values provided by the expansions around nearby points provides a rough estimate of the expansion error.

The use of several points in the α-plane connects the proposed approach with another alternative, namely the construction of a spline-approximation of the dependence of A^* and Θ^* on $H_0(x)$ and $P_0(x)$. Notice however that this alternative requires the evaluation of the homogenized coefficients at many points in the α-plane, each new point involving a new matrix, while in our approach all derivatives are obtained from the same matrix. The best choice is probably a combination of the two approaches, namely a Hermite or Padé approximation in the α-plane based on the information of high-order derivatives at several points. Our calculations above follow a simpler pro-cedure, from the six expansions the one corresponding to the *closest* point is used.

The advantages of the proposed method based on Taylor expansions are, to conclude,

(1) full decoupling of global problem from local ones;
(2) feasibility, due to the savings in computer cost, of treating general type of roughness functions;
(3) and straightforward implementation of Newton-Raphson iterations for the global problem.

The second point becomes especially relevant when the roughness is strongly anisotropic and not aligned with the flow.

References

[1] Bayada, G. and Chambat, M. (1989). Homogenization of the Stokes system in a thin film flow with rapidly varying thickness. *RAIRO Modél. Math. Anal. Numér.*, **23**(2), 205–234.
[2] Bayada, G. and Faure, J. B. (1989). A double scale analysis approach of the Reynolds roughness. comments and application to the journal bearing. *ASME Journal of Tribology*, **111**, 323–330.
[3] Bensoussan, A., Lions, J. L. and Papanicolaou, G., *Asymptotic Analysis for Periodic Structures*. North-Holland, 1978.
[4] Burgdorfer, A. (1959). The influence of the molecular mean free path on the performance of hydrodynamic gas lubricated bearings. *ASME Journal of basic Engineering*, **81**, 99–100.
[5] Buscaglia, G. and Jai, M. (2000). Sensitivity analysis and taylor expansions in numerical homogenization problems, *Numer. Math.*, **85**, 49–75.
[6] Jai, M. (1995). Homogenization and two-scale convergence of the compressible Reynolds lubrication equation modeling the flying characteristics of a rough magnetic head over a rough rigid-disk surface. *Math. Modeling and Numer. Anal.*
[7] Jikov, V. V., Kozlov, S. M. and Oleinik, O. A. (1994). *Homogenization of Differential Operators and Integral Functionals*, Springer-Verlag.

[8] Mitsuya, Y. and Ota, H. (1991). Stiffness and damping of compressible lubricating films between computer flying heads and textured media: Perturbation analysis using the finite element method. *ASME Journal of Tribology*, **113**, 819–827.

[9] Weng, C.-I., Li, W. and Hwang, C.-C. (1996). Rougness effects on dynamic coefficients of ultra-thin gas film in magnetic recording. *Transactions of the ASME*, **118**, 774–782.

[10] Ohkubo, T., Mitsuya, Y. and Ota, H. (1989). Averaged Reynolds equation extended to gas lubricant possessing surface roughness in the slip flow regime: Approximate method and confirmation experiments. *ASME Journal of Tribology*, **111**, 495–503.